

Dynamical Evolution of the Shock Cone around $4D$ Einstein-Gauss Bonnet Rotating Black Hole

O. DONMEZ*

ABSTRACT

In this paper, a Bondi-Hoyle accretion onto the rotating black hole in Einstein-Gauss Bonnet gravity is studied. By injecting the gas from upstream region of the computational domain, we have found occurrence of the stable shock cones in the downstream region. The dynamical structures and oscillation properties of these shock cones strongly depend on the black hole spin parameter a and Gauss-Bonnet coupling constant α . It is found that the various values of α can lead the different amounts of matter to pile up close to the black hole horizon, higher α causes bigger oscillation amplitude in the mass accretion rate, and the required time to reach the steady state is getting smaller with the increasing in α . Moreover, increasing α in the negative direction causes a decrease in the shock opening angle and this angle slightly increases with the increasing α in the positive direction. We found that the negative values of Gauss-Bonnet coupling constant are more favored to have interesting physical outcomes such as accretion rate and oscillation. In addition, the higher the black hole rotation parameter a emerges the higher the accretion rate. It is also confirmed that, for $\alpha \rightarrow 0$, the black hole solution in EGB gravity converges to Kerr in general relativity. Furthermore, Gauss-Bonnet coupling constant could be used to constrain the size of observed shadow of $M87^*$ radius for various values of black hole rotation parameter.

Keywords: rotating black hole, EGB gravity, shock cone, numerical relativity

1. INTRODUCTION

Understanding the nature of strong gravity using the observational and theoretical tools is still an ongoing process. After the general theory of the relativity was formulated by Einstein, many alternative theories of the gravity were proposed. The observation of $M87^*$ super-massive black hole by the Event Horizon Telescope (*EHT*) collaboration was the first direct evidence of the strong gravitational regime ([Event Horizon Telescope Collaboration et al. 2019a,b,c,d,e](#)). The observed $M87^*$ black hole shadow indicates that the observed data is well consistent with the prediction of the general theory of relativity and the black hole parameters were estimated from the shadow ([Kumar & Ghosh 2020a](#)). On the other hand the observed shadow has opened a window to have a deep understanding of the strong gravity not only in the general relativity but also in alternative theories of gravity. The alternative theories prove the existing of Kerr black hole and might be used to constrain the parameter space of the black hole using EHT collaboration data ([Kumar & Ghosh 2020b](#); [Shaikh et al. 2021](#); [Bambi et al. 2019](#)).

A wind accretion from the X -ray binary is an important physical phenomena to reveal properties of the black hole such as its spin and mass. The simplest accretion scenario occurring in the X -ray binaries is called Bondi-Hoyle-Lyttleton (BHL) accretion ([Bondi & Hoyle 1944](#)). BHL is one of the accretions studied during many decades using the tools in Newtonian and general relativistic hydrodynamics. Using the Newtonian hydrodynamics, firstly, the numerical simulation in $2D$ for an axisymmetric accretion flow was performed for adiabatic gas by [Hunt \(1971\)](#). Later, the analytic study of the accretion flow onto the compact object and estimation of the accretion rate were computed by [Davies & Pringle \(1980\)](#). There were other studies in $2D$ and $3D$ accomplished recently ([Foglizzo et al. 2005](#); [Blondin 2013](#); [MacLeod & Ramirez-Ruiz 2015](#); [Ohsugi 2018](#); [Xu & Stone 2019](#)). BHL accretion around the black hole was extensively studied using the general relativistic hydrodynamics and magneto-hydrodynamics either in case of spherical symmetry or axial symmetry ([Dönmez et al. 2011](#); [Penner 2011](#); [Dönmez 2012](#); [Penner 2012](#); [Lora-Clavijo & Guzmán 2013](#); [Lora-Clavijo et al. 2015](#); [Cruz-Ororio & Lora-Clavijo 2016](#)). Studying BHL accretion onto the rotating black hole using the modified gravity may specify more information about the rotating black hole.

A newly discovered $4D$ Einstein-Gauss-Bonnet (EGB) gravity opened a new window to define a black hole in EGB gravity. This new discovery, which contains static and spherically symmetric black hole, was used to extract important features of the astrophysical phenomena in different aspect. Number of work have been done to reveal the properties of the astrophysical system. Physical properties of the black hole ([Konoplya & Zinhailo 2020](#); [Roy & Chakrabarti 2020](#)), the gravitational lensing by the black hole ([Islam et al. 2020](#)), Hawking radiation of the massless scalar ([Zhang et al. 2020](#)), the observational limits on

* College of Engineering and Technology, American University of the Middle East, Kuwait

the Gauss-Bonnet coupling constant (Feng et al. 2020; Clifton et al. 2020), the radiating black holes (Ghosh & Maharaj 2020; Ghosh & Kumar 2020; Liu & Zhang 2021), the last stable circular orbit for photons and particles (Guo & Li 2020; Zhang et al. 2020), the non-relativistic matter perturbations growth rate (Haghani 2020) were extensively studied. In addition, the rotating black hole in EGB gravity were studied to investigate Gauss-Bonnet coupling constant α on the size of shadow in the context of massive black hole observation $M87^*$ (Kumar & Ghosh 2020b; Wei & Liu 2020), to find energy extraction efficiency for particle (Liu & Zhang 2021), and to extract the center of mass energy of the two colliding particles (Naveena Kumara et al. 2020).

After rescaling of Gauss-Bonnet coupling constant α , this constant makes a non-trivial contribution to the gravitational dynamics in a strong gravitational region. This important feature of EGB gravity starts to pay attention to understand the effects of α to different astrophysical problems around the black hole. In Donmez, Orhan (2021) they explored the properties of the shock cone in a strong gravitation region around the non-rotating black hole in EGB gravity. The cone was produced as a consequence of the Bondi-Hoyle accretion and was connected to the black hole horizon on the downstream side of the computation domain. It was found that the Gauss-Bonnet coupling constant α plays an important role not only in the creation of a shock cone but also in its oscillation properties. Increasing α caused strong oscillations inside the shock cone. These strong oscillations would lead to the Quasi-Periodic Oscillations (QPOs). Besides, they also studied the effects of the bigger α values in the negative direction and found that the oscillation amplitude of the shock cone would be suppressed.

In this paper, we study the properties of the shock cones and their oscillation properties in case of the Bondi-Hoyle accretion on the equatorial plane around the rotating black hole in EGB gravity. We numerically model the Bondi-Hoyle accretion to explore the effects of the black hole rotation parameter a and Gauss-Bonnet coupling constant α onto the shock cone dynamics. For this, we have done systematic work to find out the shock cone structures using different values of a and α . In particular, we calculate the mass accretion rate and QPOs to understand the dynamical structure of the shock cone and its oscillatory behavior as a function of a and α . We have also constrained the Gauss-Bonnet coupling constant α for the recent discovery, super-massive black hole $M87^*$. in EGB gravity and general relativity. The possible effects of both constant (a, α) on the oscillation properties of the shock cones are extensively explored.

The plan of the paper is as follows: The brief summary of recently proposed the rotating black hole in 4D EGB gravity and real solutions for various values of α and black hole spin a are summarized in Section 2. In Section 3, the general form of General Relativistic Hydrodynamical (GRHD) equations on equatorial plane, initial conditions for primitive variables, black hole spin parameter, Gauss-Bonnet coupling constant, and useful formulas to demonstrate the numerical results are described. In Section 4, the Bondi-Hoyle accretion onto the rotating black hole in EGB gravity are extensively presented. The different aspects of the numerical results for varying values of α and a are discussed computing the mass accretion rates and the power density spectra inside the shock cones. In addition, a possible application of our numerical result to the observed $M87^*$ black hole shadow is speculated. The summary and some concluding remarks are given in Section 5. The geometrized unit is studied throughout the paper, $G = c = 1$.

2. ROTATING BLACK HOLE SOLUTION OF 4D EGB GRAVITY

The non-rotating static black hole solution in 4D EGB gravity was defined by rescaling Gauss-Bonnet coupling constant $\alpha \rightarrow \alpha/(D-4)$ in the limit $D \rightarrow 4$ Glavan & Lin (2020) and it is given as;

$$ds^2 = -f(r)dt^2 + \frac{1}{f(r)}dr^2 + r^2d\theta^2 + r^2\sin(\theta)d\phi^2, \quad (1)$$

where

$$f(r) = 1 + \frac{r^2}{2\alpha} \left(1 - \sqrt{1 + \frac{8\alpha M}{r^3}} \right). \quad (2)$$

In order to generate the rotating black hole solution in 4D EGB gravity, the advance null Eddington-Finkelstein coordinates (u, r, θ, ϕ) are used with an approach (Azreg-Ainou 2014) in Eq.1 (Ghosh et al. 2020; Wei & Liu 2020). The used transformation to define the metric in Eddington-Finkelstein coordinates is

$$du = dt - \frac{dr}{f(r)}. \quad (3)$$

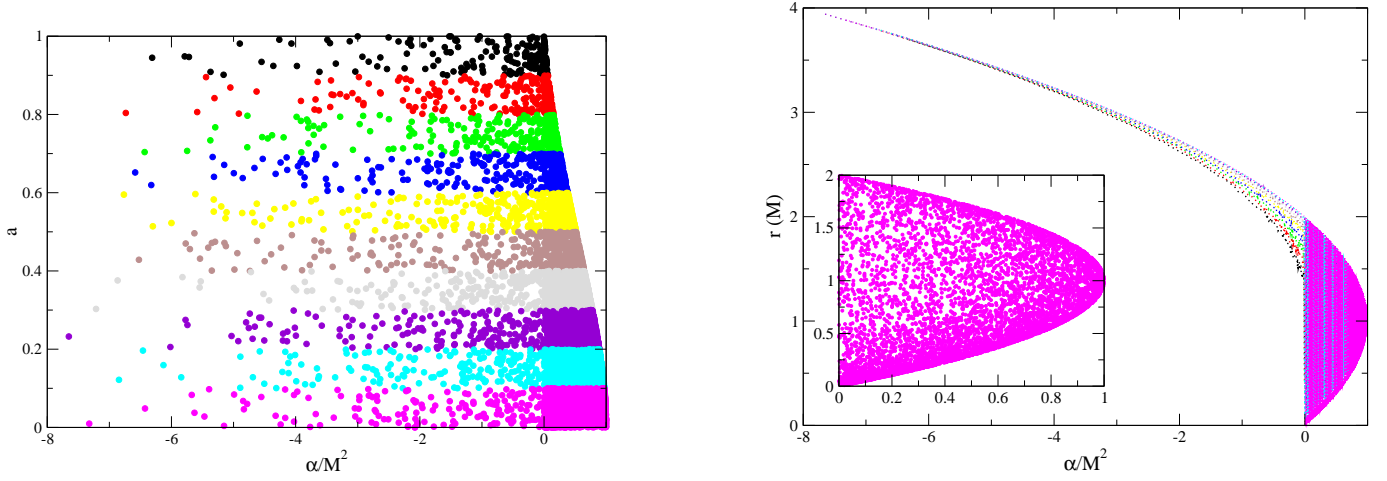


Figure 1. The existence of the black hole in EGB gravity. **Left panel:** Each point represents the parameter space (a, α) of the black hole. A less number of real solutions occur for the higher values of α in the negative direction for varying black hole spins. **Right panel:** It shows the regions for an existence of black hole space-time for various α with either degenerate horizon radius or two distinct ones.

After the statically symmetric black hole metric can be written in the advanced null coordinates, the set of the null tetrad is introduced (Ghosh et al. 2020; Wei & Liu 2020). Then radial coordinate r is defined in the complex form in the modified Newman-Janis algorithm. On the other hand, the metric functions can be represented with undefined ones which are $f(r) \rightarrow F(r, a, \theta)$ and $r^2 \rightarrow H(r, a, \theta)$. Using the transformation and finding new null tetrads, the rotating black hole metric in the Eddington-Finkelstein coordinates is given by (Ghosh et al. 2020; Wei & Liu 2020)

$$ds^2 = -Fdu^2 - 2dudr + 2a\sin^2\theta(F-1)dud\phi + 2a\sin^2\theta drd\phi + Hd\theta^2 + \sin^2\theta(H + a^2\sin^2\theta(2-F))d\phi^2, \quad (4)$$

where a is dimensionless black hole spin parameter. Using the global coordinates $du = dt' + \lambda(r)dr$ and $d\phi = d\phi' + \chi(r)dr$, Eq.4 can be written in Boyer-Lindquist coordinates. The function seen in global coordinates are $\lambda(r) = -\frac{r^2+a^2}{f(r)r^2+a^2}$ and $\chi(r) = -\frac{a}{f(r)r^2+a^2}$ (Azreg-Aïnou 2014). The undefined functions are obtained as $F = \frac{f(r)r^2+a^2\cos^2\theta}{H}$ and $H = r^2 + a^2\cos^2\theta$. Finally, the metric for the rotating black hole in EGB gravity is

$$ds^2 = -\frac{\Delta - a^2\sin^2\theta}{\Sigma}dt^2 + \frac{\Sigma}{\Delta}dr^2 - 2a\sin^2\theta \left(1 - \frac{\Delta - a^2\sin^2\theta}{\Sigma}\right) dt d\phi + \Sigma d\theta^2 + \sin^2\theta \left[\Sigma + a^2\sin^2\theta \left(2 - \frac{\Delta - a^2\sin^2\theta}{\Sigma}\right)\right] d\phi^2, \quad (5)$$

where Σ and Δ read as,

$$\begin{aligned} \Sigma &= r^2 + a^2\cos^2\theta \\ \Delta &= r^2 + a^2 + \frac{r^4}{2\alpha} \left(1 - \sqrt{1 + \frac{8\alpha M}{r^3}}\right), \end{aligned} \quad (6)$$

where a , α , and M are spin parameter, Gauss-Bonnet coupling constant, and mass of the black hole, respectively. The horizons of the black holes were obtained numerically by solving $\Delta = 0$ and given in Fig.1. Each dot on both figures represents the real solutions for various values of α and black hole spin a .

3. GENERAL RELATIVISTIC HYDRODYNAMICAL EQUATIONS, INITIAL AND BOUNDARY CONDITIONS

The General Relativistic Hydrodynamics (GRH) can be written in terms of conservations of the mass and energy-momentum

$$\begin{aligned}\nabla_a T^{ab} &= 0, \\ \nabla_a(\rho u^a) &= 0,\end{aligned}\tag{7}$$

where T^{ab} is the stress-energy-momentum tensor, u^a is the four-velocity of the fluid, and ρ is the rest-mass density of the fluid. The stress-energy-momentum tensor for perfect fluid is

$$T^{ab} = \rho h u^a u^b + P g^{ab},\tag{8}$$

where enthalpy is $h = 1 + \epsilon + \frac{P}{\rho}$. ϵ , P , and g^{ab} are the specific internal energy, pressure, and the inverse of the space-time metric, respectively.

The flux-conserving form of Eq.7 can be written using 3 + 1 formalism which are

$$\begin{aligned}\partial_t(\sqrt{\gamma}W\rho) + \partial_i((\tilde{\alpha}v^i - \beta^i)\sqrt{\gamma}W\rho) &= 0 \\ \partial_t(\sqrt{\gamma}\rho W^2 h v_j) + \partial_i((\tilde{\alpha}v^i - \beta^i)\sqrt{\gamma}\rho W^2 h v_j + \tilde{\alpha}\sqrt{\gamma}P\delta_j^i) &= \tilde{\alpha}\sqrt{\gamma}T^{ab}g_{bc}\Gamma_{aj}^c \\ \partial_t(\tau) + \partial_i((\tilde{\alpha}v^i - \beta^i)\tau + \tilde{\alpha}\sqrt{\gamma}Pv^i) &= \tilde{\alpha}\sqrt{\gamma}(T^{a0}\partial_a\tilde{\alpha} - \tilde{\alpha}T^{ab}\Gamma_{ab}^0),\end{aligned}\tag{9}$$

where the energy conserved variable $\tau = \sqrt{\gamma}(\rho h W^2 - P - W\rho)$, $\partial_t = \frac{\partial}{\partial t}$, and $\partial_i = \frac{\partial}{\partial x^i}$. v^i is three-velocity of the fluid. The indices a, b, c , and d run from 0 to 3 and Latin indices i and j run from 1 to 3. The 4- dimensional Christoffel symbol is $\Gamma_{ab}^c = \frac{1}{2}g^{cd}(\partial_a g_{bd} + \partial_b g_{ad} - \partial_d g_{ab})$. The 4- velocity components are related to 3-velocity with the following expression $u^i = W(v^i - \beta^i/\tilde{\alpha})$. The four metric g_{ab} , its inverse g^{ab} , Christoffel symbol Γ_{ab}^c , lapse function $\tilde{\alpha}$, and shift vector β^i are defined on the equatorial plane by using the metric for the rotating black hole in EGB gravity given in Eq.5.

The lapse function $\tilde{\alpha}$ is,

$$\tilde{\alpha} = \sqrt{\frac{a^2(1 - f(r))^2}{r^2 + a^2(2 - f(r))} + f(r)}\tag{10}$$

where $f(r)$ is given in Eq.2. And the shift vectors are,

$$\begin{aligned}\beta_r &= 0, \\ \beta_\phi &= \frac{ar^2}{2\pi\alpha} \left(1 - \sqrt{1 + \frac{8\pi\alpha M}{r^3}} \right), \\ \beta_\theta &= 0.\end{aligned}\tag{11}$$

The High Resolution Shock Capturing (HRSC) scheme is used to solve Eq.9 along with Marquina fluxes, and MUSCL left and right states of the primitive variables at each cell center (Dönmez 2004; Donmez 2006; Dönmez 2012).

The numerical simulation is performed in polar coordinate (r, ϕ) in the vicinity of the black hole at the center, assuming spherical symmetry. The detailed information about the code can be found in Dönmez (2004); Donmez (2006). To study the Bondi-Hoyle accretion towards the rotating black hole in EGB gravity, the velocity components of initial flow at upper boundary are given as

$$\begin{aligned}V^r &= \sqrt{\gamma^{rr}}V_\infty \cos(\phi) \\ V^\phi &= -\sqrt{\gamma^{\phi\phi}}V_\infty \sin(\phi)\end{aligned}\tag{12}$$

where V_∞ represents the asymptotic velocity at infinity. We let the gas fall towards the black the black hole homogeneously by choosing these velocities. In order to understand the effects on Gauss-Bonnet coupling constant α and black hole spin parameter

Table 1. α is Gauss-Bonnet coupling constant, a is the dimensionless black hole rotation parameter, r_{in} is the inner radius of computational domain, t_s (saturation time) is the time to reach the quasi-steady state, and $\Delta\Phi = |A_{\max} - A_{\min}|$ measures the distance between a crest and a trough.

$\alpha(M^2)$	a	$r_{in}(M)$	$t_s(M)$	$\Delta\Phi$
0.253	0.7	2.0	~ 1088	24.48
0.31599	0.644	1.7	~ 1235	17.91
0.757	0.28	2.0	~ 1086	43.37
-5.16	0.9	3.7	~ 937	30.2
-1.691	0.768	2.7	~ 1288	27.8
-0.345	0.9	2.1	~ 1009	24.2
0.000625	0.9	1.9	~ 996	27.8
0.054	0.9	1.8	~ 995	24.8
0.9997	0.0048	1.7	~ 1510	39.96
-0.422	0.952	2.2	~ 900	20.89
-2.924	0.967	3.2	~ 958	34.5
-4.9041	0.616	3.7	~ 978	34.5
-4.93	0.28	3.7	~ 1415	29.72
-3.03	0.28	3.7	~ 1338	40.28
-0.99	0.28	3.7	~ 1307	41.88
-0.37	0.28	3.7	~ 1159	38.19
0.096	0.28	3.7	~ 1093	40.65
0.41	0.28	3.7	~ 1073	40.35
0.68	0.28	3.7	~ 1039	38.90
Kerr Black Hole				
-	0.28	2.2	~ 1140	39.03
-	0.73	2.0	~ 973	24.97

a onto the shock cones, we fixed the values of asymptotic velocity $V_\infty = 0.3$, the sound speed $c_{s,\infty} = 0.1$, and adiabatic index $\Gamma = 4/3$. More detailed information about handling the initial conditions and other details can also be found in [Donmez, Orhan \(2021\)](#).

The computation domain is defined on the equatorial plane in polar coordinate and physical boundaries are located at $r_{min} \leq r \leq 100M(10r_{acc})$ and at $0 \leq \phi \leq 2\pi$. The accretion radius is

$$r_{acc} = \frac{M}{c_\infty^2 + V_\infty^2}. \quad (13)$$

In order to reduce the effect of the outer boundary, it should be located at least $4r_{acc}$. It is at $10r_{acc}$ in all our numerical simulations. As seen in Table 1, r_{min} can vary from model to model which is chosen very close the event horizon of the black hole. We divided the physical domain to the uniform cells using 1024 points along r and 512 points at ϕ directions.

We use the second-order numerical scheme so that we need to define two ghost zones at the inner and outer boundaries of the computational domain along the r . These zones are filled by copying the corresponding values from the first interior data inside the physical domain. The adopted boundary along the ϕ direction is the periodic boundary condition.

In order to understand the dynamical behavior of accretion disk in the case of Bondi-Hoyle accretion, the mass accretion rate onto the black hole is computed, assuming that the spherical detector is located close to the event horizon. The expression of the mass accretion rate is

$$\frac{dM}{dt} = - \int_0^{2\pi} \tilde{\alpha} \sqrt{\gamma} \rho u^r d\phi. \quad (14)$$

Although the accreted mass into the black hole would increase its mass a very small amount, It is fair to assume that the black hole mass is constant during evolution.

The angular momentum transfer would reveal some features of the shock cone dynamics. In order to understand the relationship between the rotating accreted matter and black hole parameters (a, α) , we compute the angular momentum flux at the inner boundary of the domain very close the black hole horizon along the spherical surface. The azimuthal component of the angular momentum flux on the equatorial plane is

$$\frac{dL}{dt} = - \int_0^{2\pi} \tilde{\alpha} \sqrt{\gamma} \rho h u^r u^\phi d\phi. \quad (15)$$

One of our main goals is to find out how the oscillating shock cone transport the angular momentum through the disk; radially outward or inward and its dependencies to the Gauss-Bonnet coupling constant and black hole rotation parameter..

4. THE ACCRETION ONTO 4D EGB ROTATING BLACK HOLE

Here, we basically focus on the dynamical evolutions of the shock cones and their oscillation properties around the rotating black hole in EGB gravity. The accretion is generated by Bondi-Hoyle accretion injecting gas from upstream region of the computational domain toward the black hole. The shock cone appears at the downstream region with a rigid opening angle. In order to extract the physical properties of these cones, we compute and plot the mass accretion rates, angular momentum accretion rate, shock cone opening angles, oscillation amplitudes of the matter inside the cone, and power spectrum density for varies values of Gauss-Bonnet coupling constant α and black hole spinning parameter a . Some of the important parameters used in numerical simulations and extracted from the calculations are given in Table 1.

4.1. Numerical Results and Discussion

In Fig.2, the color plot of the rest mass-density with their density counter is shown on the equatorial plane around the rotating black hole $a = 0.9$ in EGB gravity for different values of Gauss-Bonnet coupling constant α at $t \sim 12000M$, much later than the time to require to reach the saturation point, $\sim 1000M$. The shock cones are formed and bent around the black hole due to the warped space-time around the rotating black hole. The bended space-time is more clearly seen in case at which the inner boundary of the computation domain is more closer to the black hole. The rest-mass density is high at the inner boundary close to the back hole horizon. As it is seen in left snapshots $\alpha = 0.000625$ and $\alpha = -0.345$, having a higher rest-mass density does not only depend on the inner boundary location but it also slightly changes with α . Even though the inner boundary for $\alpha = 0.000625$ is closer to the horizon than $\alpha = -0.345$, the rest mass-density is relatively higher for $\alpha = -0.345$. The higher density could cause the hotter shock cone so that we may expect the higher energetic phenomena close the black hole horizon for different values of α .

For the different values of Gauss-Bonnet coupling constant α and black hole rotation parameter a with the same initial setup, in the numerical simulations, the major differences appear not only in the maximum saturation value of mass accretion rate but also in the oscillation property. Fig.3 shows the mass accretion rate as a function of time for different values of α and a . The values of α in first model is almost same as a in the second model. While larger a emerges a higher accretion rate computed at location $r = 6.5M$, higher α causes a bigger oscillation amplitude in the mass accretion rate. The bigger gradient in the mass accretion rate, after the shock cone reaches to the steady state, would lead to a more chaotic radiation in observed phenomena.

In Fig.4, the mass accretion rates for two sets of data are reported. The rates are plotted after they reach to the steady accretion state. The mass accretion rate has different dependency on the Gauss-Bonnet coupling constant α and the black hole rotation parameter a . As it seen from this figure, there is no striking difference between the models and they show the same type of behavior with a small gradient during the evolution in given models eventhough the inner radius of these two cases do not equal to each other. Table 1 shows that the black hole shadow radius is bigger for the model $\alpha = -1.691$ and $a = 0.768$. It might show us that the same physical situation could be reached for different values of α and a . Although the observed shadow for $M87^*$ (Event Horizon Telescope Collaboration et al. 2019a,b) is consistent with numerical results in the general relativity, we still have some open doors to find a relation between black hole rotation parameter and parameters in modified gravity for the observed $M87^*$ (Kumar & Ghosh 2020b). So that the black hole shadow diameter could be constrained with Gauss-Bonnet coupling constant α to get consistency between the numerical simulation and observation. It is shown from the numerical simulations that the model, $\alpha = -1.691$ and $a = 0.768$, with a smaller black hole rotation parameter and a bigger shadow radius could be used to understand the physical properties of the observed black hole $M87^*$ by *EHT*.

In Fig.5, the extreme values of Gauss-Bonnet coupling constant $\alpha < -2$ and the black hole rotation parameter $a > 0.6$ produce more chaotic motions in the mass-accretion rate when it is compared with the results given in Figs.3 and 4. It may be associated with the effect due to the coupling between fastly rotating black hole parameter and bigger values of α . Larger the values of

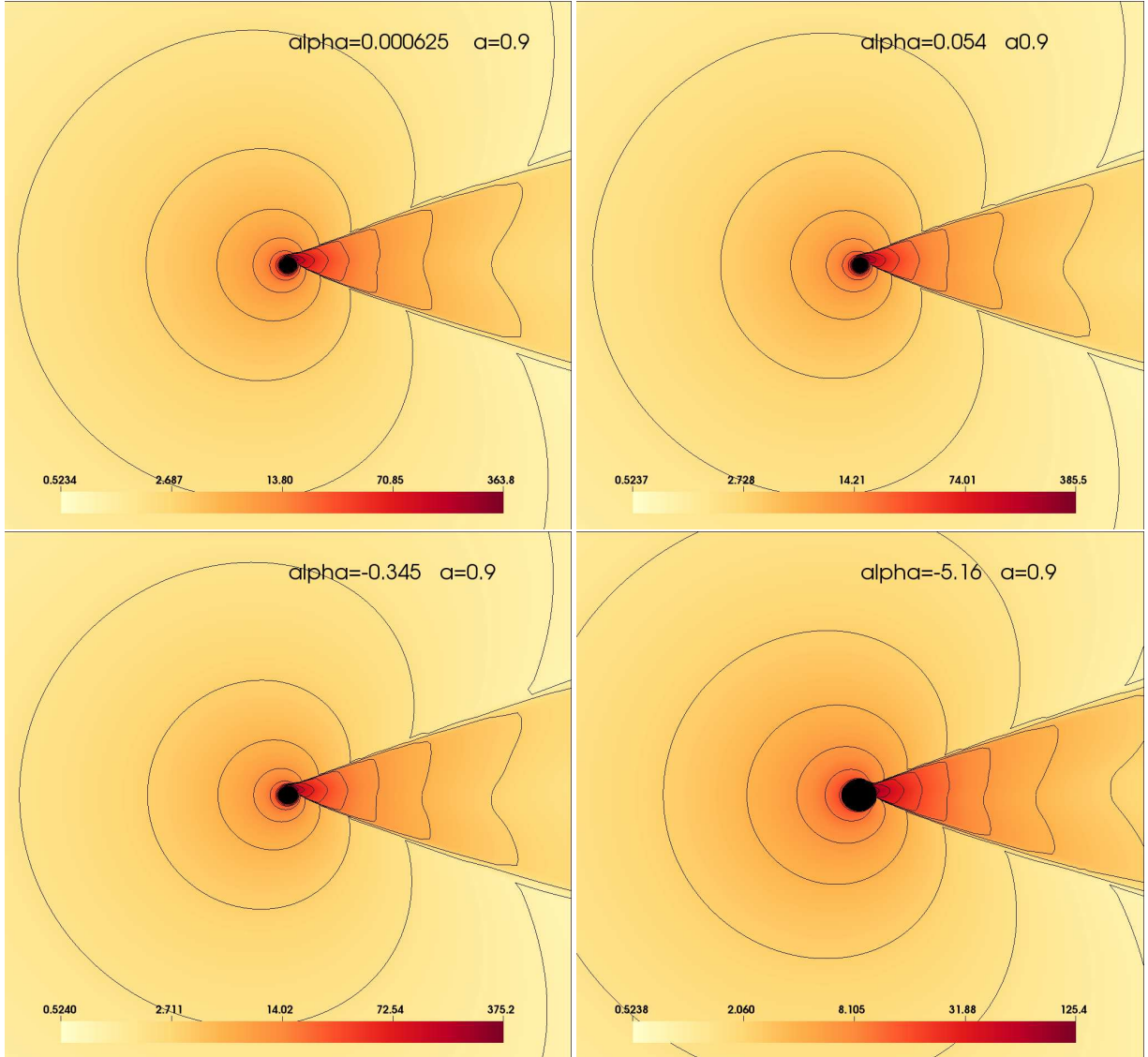


Figure 2. The logarithmic rest-mass density on the equatorial plane around the rotating black hole $a = 0.9$ in EGB gravity. The close-up view of the snapshots are plotted at much later than the shock cone reached to the steady-state. The color contour plots show the shock cone dynamics for varying values of Gauss-Bonnet coupling constant α and the close-up view boundaries are located at $[x, y] \rightarrow [-60M, 60M]$.

these parameters produces larger the oscillation amplitude in mass accretion rate. These dependences of mass accretion rate on the black hole parameters reveal more detail effects and cause rapid growth on it. The results in Figs. 4 and 5 indicate that the negative values of α is more interesting to study to extract more details about physical system. It was also put forward by [Wei & Liu \(2020\)](#) when they were studying the rotating black hole shadow.

The Bondi-Hoyle accretion creates a steady-state shock cone around the rotating black hole. The falling gas gets toward the black hole due to the gravitational force and settles into the equatorial plane. The angular momentum of the rotating gas can play an important role in the moving of gas towards or away from the black hole. In order to measure the strength of how the angular momentum would be transferred outwards, we compute the angular momentum flux which clearly shows the effect of various values of Gauss-Bonnet coupling constant α and the black hole rotation parameter a to the shock cone dynamics, seen in Fig.6. As it is seen in upper part of Fig.6, when changing α , a difference appears in the strength of angular momentum flux for the same values of a although oscillation behavior is almost the same. The higher the α in negative direction leads the bigger in the angular momentum flux, that is, the more angular momentum would be transferred outward for $\alpha = -2.924$. It is also

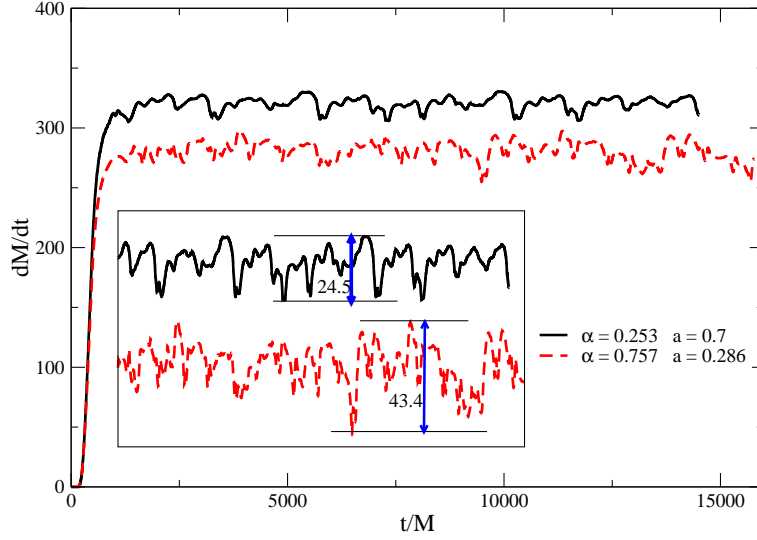


Figure 3. The comparison of the mass accretion rates for two different cases. The accretion process reaches a quasi-stationary state steady around $1200M$. While the higher the black hole spin causes the more matter to accrete towards the black hole, the oscillation amplitude gets larger for the higher positive value of the Gauss-Bonnet coupling constant α .

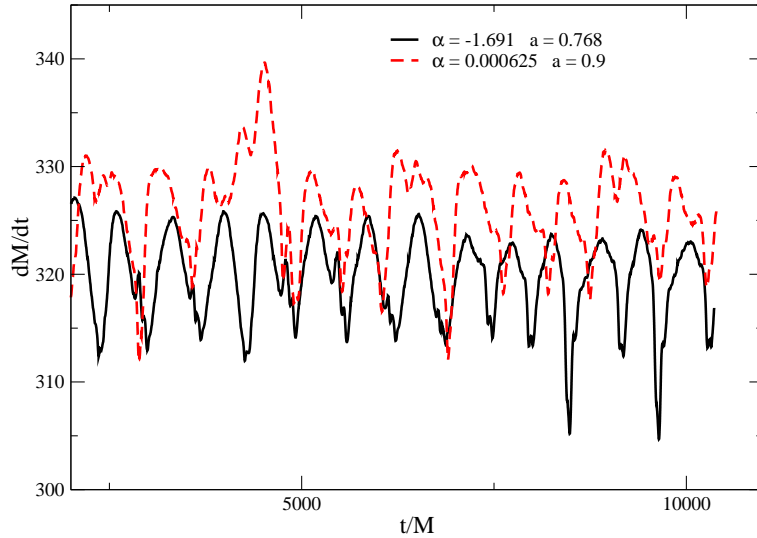


Figure 4. The same as Fig.3 but for different values of a and α . The distance between a crest and a trough is $\psi = |A_{\max} - A_{\min}| = 27.8$ in both model.

consistent with the energy extraction efficiency which increases with the larger value of α in the negative direction Liu & Zhang (2021). The angular momentum flux around the Kerr and rotating black holes in EGB gravity for two different values of α are given in the middle part of Fig.6 using the similar rotation parameter $a = 0.7$. The angular momentum flux almost oscillates around zero value while it is negative for the gas rotating around Kerr black hole. The result in EGB gravity definitely shows a deviation from the Kerr solution. We have observed the same trend in the lower part of the same figure. It is clearly seen from the simulations that the considerable amount of angular momentum (inward or outward direction) would be transferred for various values of Gauss-Bonnet coupling constant α either in negative or positive direction when it is compared with the Kerr solution in the general relativity.

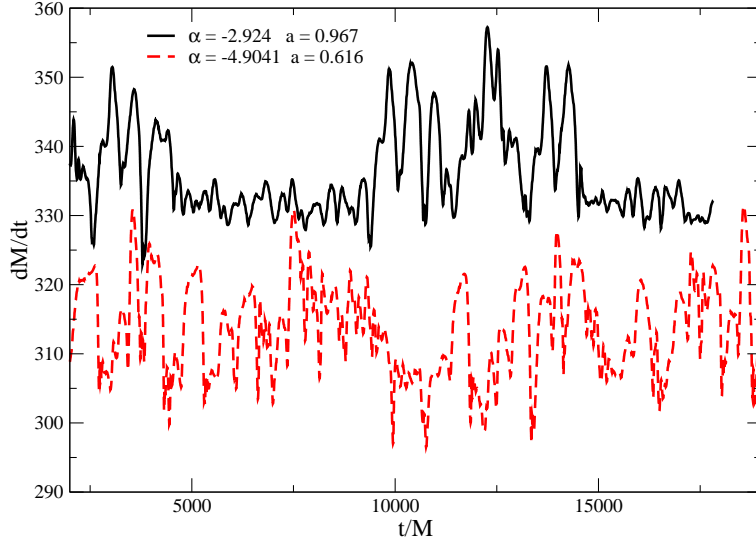


Figure 5. The same as Fig.3 but for different values of a and α . The distance between a crest and a trough is $\psi = |A_{\max} - A_{\min}| = 34.5$ in both model.

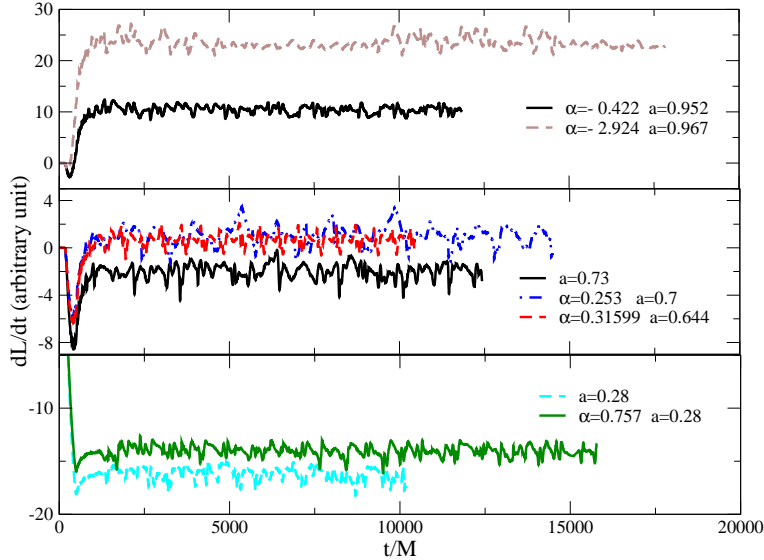


Figure 6. The comparison of the angular momentum fluxes versus time computed at the inner boundary of the computational domain for different models. The angular momentum transformation strongly depends on the black hole spin and Gauss-Bonnet coupling constant α .

In order to depict the strength of the chaotic behavior of the shock cone after reaching the steady state, we plot $\Delta\Phi$ as a function of Gauss-Bonnet coupling constant α for a fixed black hole rotation parameter $a = 0.28$ and for the inner radius $r_{in} = 3.7M$ in Fig. 7. $\Delta\Phi = |A_{\max} - A_{\min}|$ represents the distance between a crest and a trough. It is obvious from the figure that the value of $\Delta\Phi$ reaches the maximum on the left and on the right sides of α when α gets closer to 0. Moreover, the value of $\Delta\Phi$ converges to Kerr solution in general relativity when $\alpha \rightarrow 0$. It can also be seen in Table 1.

In Fig. 8, after the shock cone is accreted downstream region of the accretion flow, the cone opening angle slightly depends on Gauss-Bonnet coupling constant α for the fixed value of the black hole rotation parameter $a = 0.28$. While increasing of α in the negative direction decreases the opening angle, this angle slightly increases with the increasing of α in the positive direction. It

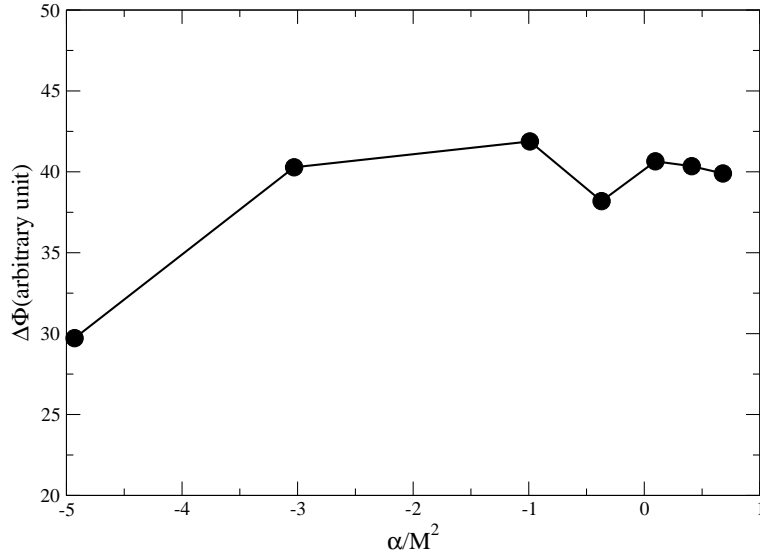


Figure 7. Dependencies of $\Delta\Phi$ versus Gauss-Bonnet coupling constant α for a fixed black hole rotation parameter $a = 0.28$ and at the radius $r_{in} = 3.7M$. $\Delta\Phi$ gets maximum values on the left and the right sides of $\alpha \rightarrow 0$ at where EGB black hole solution converges to the Kerr black hole one.

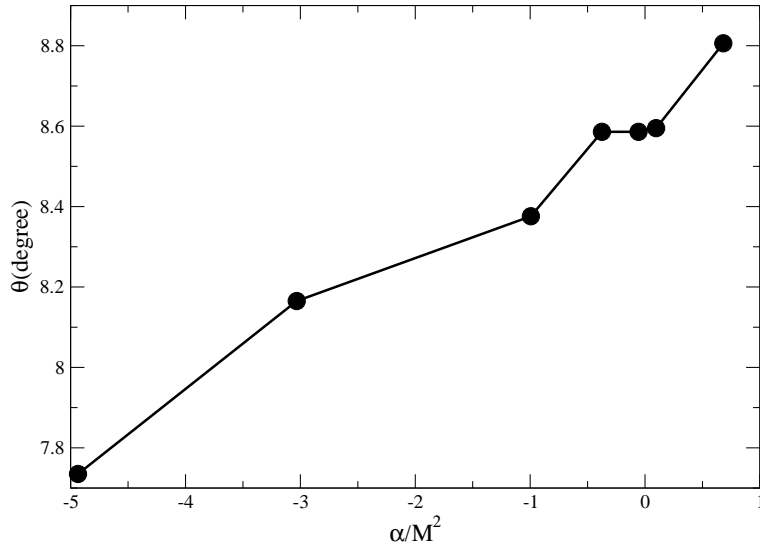


Figure 8. The dependency of the shock cone opening angle θ to the Gauss-Bonnet coupling constant α for the same initial parameters used in Fig.7.

is also seen in Fig.8 that when $\alpha \rightarrow 0$, the black hole solution in EGB gravity converges to Kerr in general relativity. It was also confirmed for the Schwarzschild solution (Donmez, Orhan 2021). In particular, as seen in Figs. 3, 4, and 5, the mass accretion rates strongly depend on α and a . In addition, the reduced shock opening angle would decrease in the accretion rate (Zanotti et al. 2011).

In order to extract more information about the availability of the shock cone and its structure due to Gauss-Bonnet coupling constant α , we compute the required time for the shock cone to go to the steady-state in Fig.9. It is also called the saturation time. According to our initial models, maximum saturation time is observed at $\alpha \sim -5$ but it gets smaller when α is increasing. The

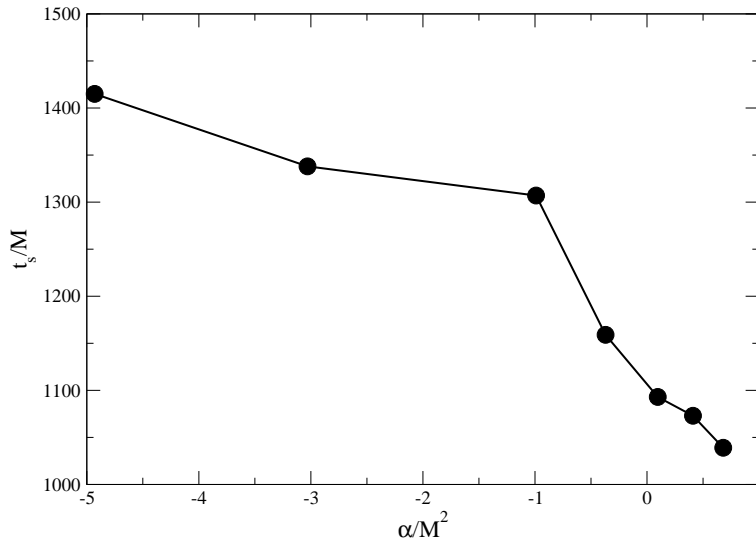


Figure 9. The time needed reach the quasi-steady-state (saturation time) versus the Gauss-Bonnet coupling constant α is plotted for the same initial parameters used in Fig.7.

same behavior was also found for the non-rotating black hole in EGB gravity (Donmez, Orhan 2021). On the other hand, it is seen in Table 1 that the saturation time in EGB gravity converges to Kerr solution in general relativity. In addition, the saturation time also depends on the black hole rotation parameter a . The higher a causes the lower the time to reach the steady state, seen in Table 1.

In Fig.10, in order to illustrate the physical properties of shock cone as functions of Gauss-Bonnet coupling constant α and black hole rotation a , we consider two different initial models. One is $\alpha = 0.9997$ with very slowly rotating black hole $a = 0.0048$ and the other one is $\alpha = 0.000625$ with a fastly rotating black hole $a = 0.9$. We found that the shock cone location is shifted to the right due to the warped space-time as a consequence of fastly rotating black hole, seen in the bottom panel of Fig.10, when it is compared with the case, smaller rotation parameter. In the upper panel of Fig.10, one can observe that the strong oscillation property can lead to more chaotic motions. These types of cases would be a good candidate to observe QPOs in the X -ray binary system. A similar behavior was also found for the thin accretion disk around the non-rotating black hole in EGB gravity (Liu et al. 2021). They indicated that the disk is hotter and more efficient than that around Schwarzschild black hole for a positive α . It is concluded that the shock cone location is mainly dependent of black hole rotation parameter a , while the wild behavior of the oscillating shock cone is dependent of Gauss-Bonnet coupling constant α . Of course, the average values of mass accretion rate for the fastly rotating black hole is 1.35 times larger than the case for very slowly rotating one.

4.2. Super-massive Black Hole M87*

The existence of super-massive black hole at the center of galaxy M87 has been observed using the very large baseline interferometer (Event Horizon Telescope Collaboration et al. 2019a,b,c,d,e). The observed M87* black hole shadow indicates that the observed data is well consistent with the prediction of the general theory of relativity. The event horizon telescope collaboration found the black hole mass as $M87^* = (6.5 \pm 0.7) \times 10^9 M_\odot$. The calculated Schwarzschild radius of the black hole is $R = 5.9 \times 10^{-4}$ parsecs. The range of the radius can be defined in terms of the black hole mass, $R = (1.899 \pm 0.206)M87^*$. The estimated rotation parameter is $a = 0.9 \pm 0.1$. It is consistent with the numerical simulations found by using the numerical hydrodynamics with Kerr space-time metric (Event Horizon Telescope Collaboration et al. 2019a,b,c,d,e). The black hole shadow diameter was determined by the black hole mass-distance ratio and orientation of the black hole spin axis. But many other effects were not considered which might also influence the the black hole diameter, such as the magnetic filed of the accretion flow (Narayan et al. 2012), the electron heating and colliding processes (Chael et al. 2018; Davelaar et al. 2019), misalignment between black hole spin and jet (Vincent et al. 2021).

In addition to the effects of the general relativity, the black hole shadow diameter could be influenced by Gauss-Bonnet coupling constant α in EGB gravity. Our numerical results show that Gauss-Bonnet coupling constant could be used to constrain M87* radius for various values of black hole rotation parameter. Constrained Gauss-Bonnet constant should be $-1.7 < \alpha < \sim 0.35$ and

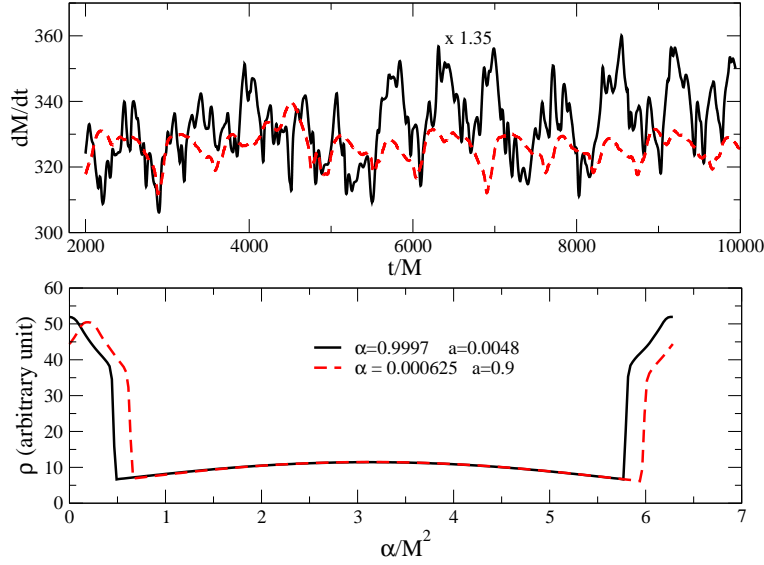


Figure 10. Comparisons of the mass accretion rates after they have reached to the steady-state and the rest-mass densities along the angular direction at $r \sim 6.5M$. We compare the numerical results between the highest possible value of positive α with the smallest rotation parameter and the smallest possible value of positive α with a fastly rotating black hole.

the black hole rotation parameter a and black hole radius would vary depending on Gauss-Bonnet coupling constant as seen in Table.1. As a consequence, the possible size of black hole shadow would be possible for varying positive or negative α (Guo & Li 2020). The negative Gauss-Bonnet constant α can break the universal bounds on the size of the black hole proposed in Lü & Lyu (2020).

4.3. QPOs around the Black Hole in EGB gravity

The matter around the black hole is piled up due to the strong gravity and causes strong collisions between gas molecules. So that the accreted material is heated to high temperatures and QPOs would be created. In the observed X -ray fluxes, QPOs are commonly observed and they can be used to extract the black hole properties, such as mass and spin indirectly.

The studying the QPOs in Fourier domain allows us to study the oscillation properties of accreted matter and shock cone close to the black hole. So that we can deduce the connections between oscillating shock and Gauss-Bonnet coupling constant α . The mass-accretion rate data is used to obtain the power spectra for different values of α and Kerr black hole, seen in Figs.11 and 12. There is a distinct behavior in the power spectra between Figs.11 and 12 computed inside the shock cone. The mode found in the numerical solutions are global eigenmodes which occur in the oscillating shock cone since the power spectra does not depend on the radial position. In Fig.11, the genuine eigenmodes and their nonlinear couplings are shown for the negative values of α , while these modes for positive values of α and Kerr black hole are given in Fig.12. For $\alpha = -4.93$, $f_1 = 6.1$ Hz and $f_2 = 12.9$ Hz are genuine modes, while $f_1 + f_2 = 19.7$ Hz and $f_1 + 2f_2 = 33.2$ Hz are the nonlinear coupling of those genuine modes with a 1.2 Hz of error bar. For $\alpha = -3.03$, $f_1 = 9.7$ Hz and $f_2 = 14.9$ Hz are genuine modes, while $f_1 + f_2 = 24.5$ Hz, $2f_1 + f_2 = 34.26$ Hz, and $f_1 + 2f_2 = 42$ Hz with a 2 Hz of error bar. For $\alpha = -0.99$, $f_1 = 5.5$ Hz and $f_2 = 15.2$ Hz are genuine modes, while $f_1 + f_2 = 21.6$ Hz, $2f_2 = 30.7$ Hz, $f_1 + 2f_2 = 35$ Hz, and $2f_1 + 2f_2 = 40$ Hz with a 1 Hz of error bar. For $\alpha = -0.37$, $f_1 = 8.2$ Hz and $f_2 = 12.2$ Hz are genuine modes, while $f_1 + f_2 = 18.8$ Hz, $2f_2 = 23.2$ Hz, $f_1 + 2f_2 = 33.9$ Hz, $f_1 + 3f_2 = 43$ Hz, and $f_1 + 4f_2 = 55.7$ Hz with a 2 Hz of error bar. For the shock cone around the Kerr black hole, $f_1 = 14.9$ Hz and $f_2 = 22.4$ Hz are genuine modes, while $f_1 + f_2 = 35.2$ Hz, $2f_2 = 47.2$ Hz, and $f_1 + 2f_2 = 64.4$ Hz with a 3 Hz of error bar. For $\alpha = 0.096$, $f_1 = 5.6$ Hz and $f_2 = 13.8$ Hz are genuine modes, while $f_1 + f_2 = 20.4$ Hz, $f_1 + 2f_2 = 32$ Hz, $3f_2 = 44$ Hz, and $4f_2 - f_1 = 50.4$ Hz with a 2 Hz of error bar. For $\alpha = 0.41$, $f_1 = 6.8$ Hz and $f_2 = 18.9$ Hz are genuine modes, while $f_1 + f_2 = 24.6$ Hz and $2f_2 = 37.9$ Hz with a 1 Hz of error bar. For $\alpha = 0.68$, $f_1 = 9.3$ Hz and $f_2 = 15.3$ Hz are genuine modes, while $f_1 + f_2 = 25.7$ Hz, $f_1 + 2f_2 = 32$ Hz, $2f_1 + f_2 = 34.8$ Hz, $f_1 + 2f_2 = 40.4$ Hz, and $f_1 + 3f_2 = 52.7$ Hz with a 2 Hz of error bar. The nonlinear couplings of modes are the expected behavior in the nonlinear physical system (Landau & Lifshitz 1976). It is found that there is a correlation between Gauss-Bonnet coupling constant α and

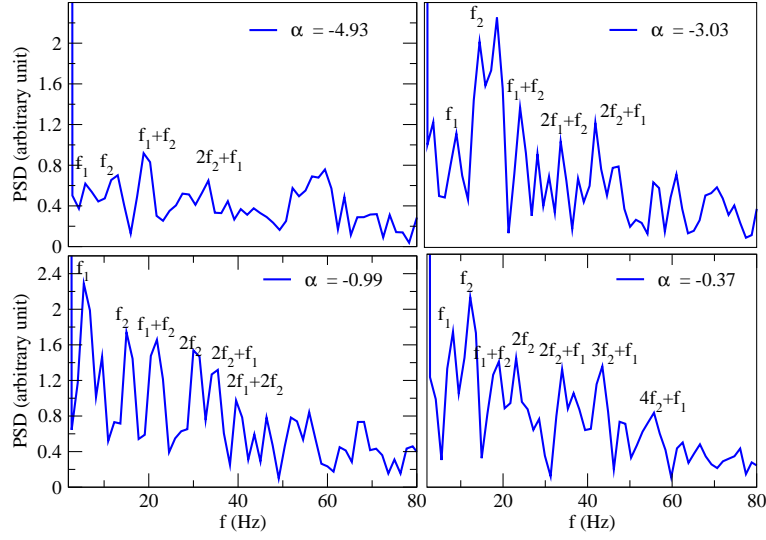


Figure 11. Power spectra is computed from the mass accretion rate dumped at $r = 6.5M$ by spherical detector for different values of Gauss-Bonnet coupling constant α around the rotating black hole in EGB gravity with $a = 0.28$. The black hole mass is chosen as $M = 10M_{\odot}$

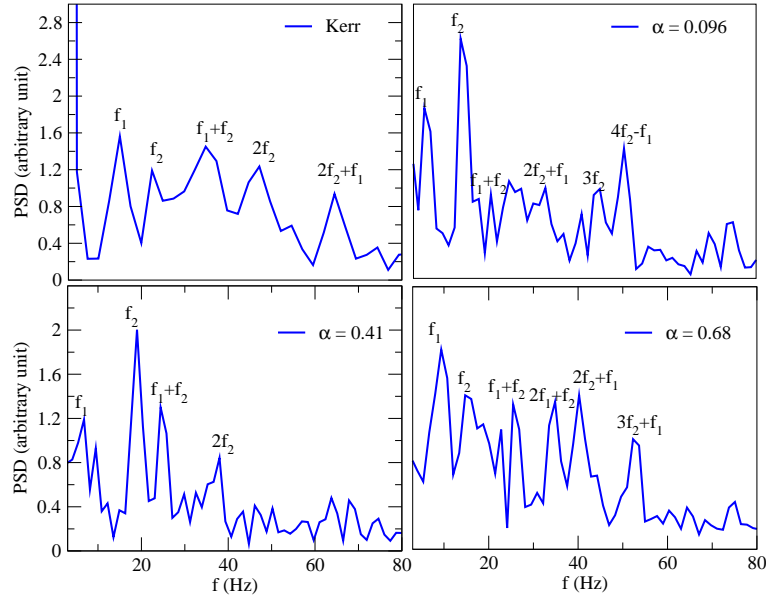


Figure 12. Same as Fig 11 but for different values of α and Kerr solution in general relativity.

genuine modes and their nonlinear coupling. The amplitude of the genuine mode is getting bigger when α approaches to zero in negative directions. It was also confirmed in the oscillation of the shock cone around the non-rotating black hole in EGB gravity [Donmez, Orhan \(2021\)](#). Similarly, the eigenmodes amplitudes are slightly larger for bigger α . The influence of α on the power eigenmodes and their nonlinear coupling is clearly seen in Figs. 11 and 12. The power spectrum density is more violent and shows more chaotic behavior for varying values of α when we compare with Kerr black hole solution with the same rotation parameter $a = 0.28$. On the other hand, the nonlinear coupling term in the highest frequency is observed in the Kerr solution.

5. CONCLUSION

We have performed a certain number of numerical simulations of the shock cone around the rotating black hole in EGB gravity by injecting the gas from the upstream region of the computational domain and by solving the GRH equations using the HRSC scheme. We have analyzed the dynamical structures of those cones and their oscillation properties that can be affected by the Gauss-Bonnet coupling constant α and black hole rotation parameter a . The negative and positive values of α with the varying a are used to understand the many physical details of these shock cones. The black hole solution in EGB gravity converges to Kerr in general relativity when $\alpha \rightarrow 0$.

We find that the more matter close the black hole is not only piled up due to the fastly rotating black hole but the different values of α also causes to it. Increasing in the amount of matter lades a chaotic motion and also causes the matter falling towards the black hole. After the shock cone reaches to the steady state, the bigger mass accretion rate gradient would lead more chaotic radiation in the observed phenomena. On the other hand, the position of shock cone is mainly dependent of the black hole rotation parameter a , while the wild behavior of the oscillating shock cone is dependent of Gauss-Bonnet coupling constant α . Increasing α in the negative direction decreases the opening angle of the shock cone, this angle slightly increases with the increasing α in the positive direction.

Together with the mass accretion rate towards the black hole, we have investigated the angular momentum rate, which is particularly important to know whether the gas moves towards or away from the black hole. Irregularities would be observed on the shock cone when the angular momentum transformation occurs. Our simulations show that the considerable amount of angular momentum (inward or outward direction) would be transferred for various values of Gauss-Bonnet coupling constant α either in negative or positive direction when it is compared with the Kerr solution in the general relativity.

We have also focused on the oscillations inside the shock cones after it reaches the steady state. The saturation times to reach the steady state are not the same in all models. The maximum saturation time is observed at $\alpha \sim -5$ and it gets smaller when α increases. On the other hand, the saturation time in EGB gravity converges to Kerr solution in general relativity. Meanwhile, the oscillation properties of the accreted matter and shock cone close to the black hole can be extracted using the Fourier transform to compute the power spectrum density . The spectrum density shows the non-linear couplings of the modes for varying values of α when we compare with Kerr black hole solution with the same rotation parameter and black hole mass.

Finally, the alternative theory of the modified gravity should not be ignored to constrain the physical properties of the observed black hole. We have carried out an indirect comparison with observed shadow of $M87^*$ black hole and found that Gauss-Bonnet coupling constant α could be used to constrain $M87^*$ radius for various values of the black hole rotation parameter a . Our numerical simulations show that the smaller a and a bigger shadow radius could be used to understand the physical properties of the $M87^*$.

ACKNOWLEDGMENTS

All simulations were performed using the Phoenix High Performance Computing facility at the American University of the Middle East (AUM), Kuwait.

REFERENCES

- Azreg-Ainou, M. 2014, PhRvD, 90, 064041
- Bambi, C., Freese, K., Vagnozzi, S., & Visinelli, L. 2019, PhRvD, 100, 044057
- Blondin, J. M. 2013, The Astrophysical Journal, 767, 135
- Bondi, H., & Hoyle, F. 1944, MNRAS, 104, 273
- Chael, A., Rowan, M., Narayan, R., Johnson, M., & Sironi, L. 2018, MNRAS, 478, 5209
- Clifton, T., Carrilho, P., Fernandes, P. G. S., & Mulryne, D. J. 2020, PhRvD, 102, 084005
- Cruz-Orsorio, A., & Lora-Clavijo, F. D. 2016, MNRAS, 460, 3193
- Davelaar, J., Olivares, H., Porth, O., et al. 2019, A&A, 632, A2
- Davies, R. E., & Pringle, J. E. 1980, Monthly Notices of the Royal Astronomical Society, 191, 599
- Dönmez, O. 2004, Ap&SS, 293, 323
- Donmez, O. 2006, AM&C, 181, 256
- Dönmez, O. 2012, MNRAS, 426, 1533
- Dönmez, O., Zanotti, O., & Rezzolla, L. 2011, MNRAS, 412, 1659
- Donmez, Orhan. 2021, Eur. Phys. J. C, 81, 113
- Event Horizon Telescope Collaboration, Akiyama, K., Alberdi, A., et al. 2019a, ApJL, 875, L1
- . 2019b, ApJL, 875, L2
- . 2019c, ApJL, 875, L3
- . 2019d, ApJL, 875, L4
- . 2019e, ApJL, 875, L5
- Feng, J.-X., Gu, B.-M., & Shu, F.-W. 2020, arXiv e-prints, arXiv:2006.16751
- Fogliizzo, T., Galletti, P., & Ruffert, M. 2005, A&A, 435, 397

- Ghosh, S. G., Kumar, A., & Singh, D. V. 2020, *Physics of the Dark Universe*, 30, 100660
- Ghosh, S. G., & Kumar, R. 2020, *Classical and Quantum Gravity*, 37, 245008
- Ghosh, S. G., & Maharaj, S. D. 2020, *Physics of the Dark Universe*, 30, 100687
- Glavan, D., & Lin, C. 2020, *PhRvL*, 124, 081301
- Guo, M., & Li, P.-C. 2020, *European Physical Journal C*, 80, 588
- Haghani, Z. 2020, *Physics of the Dark Universe*, 30, 100720
- Hunt, R. 1971, *Monthly Notices of the Royal Astronomical Society*, 154, 141
- Islam, S. U., Kumar, R., & Ghosh, S. G. 2020, *Journal of Cosmology and Astroparticle Physics*, 2020, 030
- Konoplya, R. A., & Zinhailo, A. F. 2020, *Physics Letters B*, 810, 135793
- Kumar, R., & Ghosh, S. G. 2020a, *ApJ*, 892, 78
- . 2020b, *JCAP*, 2020, 053
- Landau, L., & Lifshitz, E. 1976, *Mechanics*, 1 (Oxford: Pergamon Press)
- Liu, C., Zhu, T., & Wu, Q. 2021, *Chinese Physics C*, 45, 015105
- Liu, Y., & Zhang, X. . 2021, *Chinese Physics C*
- Lora-Clavijo, F. D., Cruz-Osorio, A., & Moreno Méndez, E. 2015, *ApJS*, 219, 30
- Lora-Clavijo, F. D., & Guzmán, F. S. 2013, *MNRAS*, 429, 3144
- Lü, H., & Lyu, H.-D. 2020, *Phys. Rev. D*, 101, 044059
- MacLeod, M., & Ramirez-Ruiz, E. 2015, *The Astrophysical Journal*, 803, 41
- Narayan, R., Sądowski, A., Penna, R. F., & Kulkarni, A. K. 2012, *MNRAS*, 426, 3241
- Naveena Kumara, A., Rizwan, C. L. A., Hegde, K., Sabir Ali, M., & M, A. K. 2020, arXiv e-prints, arXiv:2004.04521
- Ohsugi, Y. 2018, *Astronomy and Computing*, 25, 44
- Penner, A. J. 2011, *Monthly Notices of the Royal Astronomical Society*, 414, 1467
- . 2012, *Monthly Notices of the Royal Astronomical Society*, 428, 2171
- Roy, R., & Chakrabarti, S. 2020, *PhRvD*, 102, 024059
- Shaikh, R., Pal, K., Pal, K., & Sarkar, T. 2021, arXiv e-prints, arXiv:2102.04299
- Vincent, F. H., Wielgus, M., Abramowicz, M. A., et al. 2021, *Astron. Astrophys.*, 646, A37
- Wei, S.-W., & Liu, Y.-X. 2020, arXiv e-prints, arXiv:2003.07769
- Xu, W., & Stone, J. M. 2019, *MNRAS*, 488, 5162
- Zanotti, O., Roedig, C., Rezzolla, L., & Del Zanna, L. 2011, *MNRAS*, 417, 2899
- Zhang, Y.-P., Wei, S.-W., & Liu, Y.-X. 2020, *Universe*, 6, 103